EUROPEAN ORGANIZATION FOR NUCLEAR RESEARCH
CERN ACCELERATORS AND TECHNOLOGY SECTOR

CERN-ATS-2013-040

Energy Calibration of the LHC Beams at 4 TeV

J. Wenninger

Abstract

The mixed proton and lead ion run in January and February 2013 (p-Pb run) provided an excellent opportunity to measure the beam energy at the LHC. The beam energy of the LHC was determined at 4 TeV and at 450 GeV using the frequency difference of proton and lead ions by taking advantage of the simultaneous presence of both particle types in the LHC. The data for the energy measurement was collected parasitically to standard p-Pb physics operation. The measured energy at 4 TeV is $P_{4\mathrm{TeV}} = 3988 \pm 5\,(\mathrm{stat}) \pm 26\,(\mathrm{syst})\,\mathrm{GeV/c}$. The LHC energy at injection was measured with better accuracy than before to be $P_{\mathrm{inj}} = 450.28 \pm 0.01\,(\mathrm{stat}) \pm 0.11\,(\mathrm{syst})\,\mathrm{GeV/c}$. Both values are in good agreement with the predictions from the magnetic model of the LHC and the measurement accuracies are entirely dominated by systematic errors.

CERN-ATS-2013-040
01/06/2013

Geneva, Switzerland

June 1, 2013

1 Introduction

Operation of the LHC between 2009 and 2013 saw an impressive progression of the peak and integrated luminosities which culminated in the announcement of the discovery of a Higgs-like particle at a mass of 125 GeV/c^2 by the ATLAS and CMS collaborations [1, 2]. Total pp cross section measurements were performed in parallel to the standard pp physics operation using the Van de Meer scan method and special operation with high β^* by the TOTEM collaboration [3]. Important progress was made on those measurements, pushing systematic error down in the range of $2-3\%$. Following this reduction of the error on the total cross-section, the uncertainty on the LHC beam momentum can be become a significant contribution for measurement errors. At the time of writing of this document the LHC experiments have expressed the wish to know the LHC beam energy with an accuracy better than 1%.

The 12 year beam energy calibration programme of LEP was extremely successful in providing accurate beam energies between 40 and 100 GeV/c. Although resonant depolarization, the workhorse of LEP energy calibration, is not available at the LHC, the experience gained on LEP is also relevant for LHC energy calibration. In particular the studies on the ring circumference variations are important in the context of the LHC, since such affects play an important role in accurate measurements of the LHC beam energy. Based on the LEP and SPS experience with energy calibration first estimates for the expectations at the LHC were described in a note [6]. Updated numbers for energy estimates were published in 2012 in the context of a luminosity calibration workshop [7].

This report begins with a brief description of the main ingredients to the energy of a storage ring. The calibration method based on the comparison of proton and ion beams is discussed in some details, highlighting the bonus of the mixed operation mode of proton and lead ions for the measurement systematics. The measurements at 4 TeV and at injection are presented in detail together with the estimates for the systematic errors. The results are compared to estimates from magnetic model extrapolations and are used to estimate the errors that could be expected in the future at 7 TeV.

2 Beam Momentum and Magnetic Fields

In a storage ring like the LHC the average beam momentum P of each ring is defined by the integral of the bending field B along the closed orbit of each beam

$$P = \frac{Ze}{2\pi} \oint B(s)\, ds = Z \times 47.7[\mathrm{MeV/c/Tm}] \oint B(s)\, ds\ , \tag{1}$$

where Ze is the particle charge, Z = 1 for protons and Z = 82 for Pb^{82+} lead ions. s is the longitudinal coordinate along the beam orbit. The contributions of the various magnets to the beam momentum can be decomposed into 3 terms,

$$P = P_d + \Delta P_q + \Delta P_\epsilon \tag{2}$$

where P_d is the contribution of the dipoles. ΔP_q is the correction to the energy due the quadrupoles. Other elements, for example horizontal orbit correctors used for beam steering, can give additional small contributions ΔP_ϵ to the momentum. P_d depends on the integrated

dipole field $(BL)_d$ and accounts usually for almost 100% of the beam energy since the dipoles define the nominal momentum,

$$P_d = \frac{e}{2\pi}(BL)_d \ . \tag{3}$$

The relative energy change $\Delta P_q/P$ can be expressed in terms of orbit length C or alternatively RF frequency f_{RF}

$$\frac{\Delta P_q}{P} = \frac{1}{\alpha}\frac{C - C_c}{C} = -\frac{1}{\alpha}\frac{f_{RF} - f_{RFc}}{f_{RF}} \ . \tag{4}$$

It is a function of the momentum compaction factor α, $\alpha \simeq 3.2 \cdot 10^{-4}$ for the LHC, of the central orbit length (circumference) C_c or central RF frequency f_{RFc}. The central orbit length (or central RF frequency) correspond to the orbit where the beam is centered on average in the quadrupoles; on this orbit ΔP_q vanishes. In general $\Delta P_q/P$ does not account for more than few per-mill of the bending field integral. For a perfectly aligned machine the definition of the central frequency f^c_{RF} (and of the central orbit length) is unambiguous. It corresponds to the RF frequency (or orbit length) for which the beam is centered in *all* quadrupoles. In a real machine with misaligned magnets the beam is travelling on a closed orbit that is not centered in each quadrupole. In such a case the central frequency corresponds to the RF frequency for which the beam is centered *on average* in the quadrupoles.

3 Energy Calibration

3.1 Magnetic Field Calibrations

The simplest way to estimate the beam momentum is to derive it from the magnetic calibration curves of the dipole magnets (also referred to as transfer functions). The same calibration curves are used to generate the current settings of the power converters that feed the magnets during beam operation. For dipoles magnets that are measured in cold (super-conducting) conditions in SM18, the contributions to the error are given by a relative measurement accuracy of 3×10^{-4}, to which one has to add the long term reproducibility (10^{-4}) and the uncertainty on the current setting of the power converter (10^{-4}). The estimate for the total relative error is 5×10^{-4} [8]. For magnets that are not measured in cold conditions, there is an additional error of 5×10^{-4} due to the uncertainty on the correlation between cold and warm measurements. An estimate for the total relative uncertainty on the dipole field at $3.5 - 7$ TeV/c is $\sim 7 \times 10^{-4}$ [8].

3.2 Resonant Depolarization

For electron machines resonant depolarization provides a high precision measurement technique which relies on the precession frequency of the electron spins in the magnetic lattice of the storage ring. Electron beams polarize spontaneously in a ring up to a theoretical limit of 92% due to synchro radiation, and the spin precession frequency is proportional to the energy [9, 10]. Unfortunately this technique does not work for proton beams as the polarization time at the LHC is too long.

3.3 Spectrometers

Momentum measurements using spectrometer systems require a precisely calibrated and monitored dipole magnet that has to fit into the machine lattice. An open drift space of $\sim$ 10 m

is required on either side of the magnet to determine the angles with beam position monitors (BPMs). The spectrometer system usually requires precise cross calibrations with another absolute measurement technique at some energies, and is mainly used for extrapolation to the desired target energy. The difficulty at the LHC is too find a suitable location, as for practical reason the spectrometer magnet should be normal-conducting to ease the installation and maintenance of precision instrumentation to monitor the magnetic field (for example Nuclear Magnetic Resonance probes).

One of the three energy calibration techniques used at LEP2 for high beam energies consisted of such a magnetic spectrometer [10]. The core of the spectrometer was a dedicated, individually powered dipole magnet that was calibrated in a laboratory and in situ with very high accuracy. This dipole was surrounded on either side by 3 dedicated BPMs installed in a 20 meter long field-free region. The BPMs were surveyed by a wire positioning system and provided a precise relative beam angle measurements on both sides of the magnet. The BPM and alignment system resolutions were in the range of 1 μm. The magnet was equipped with in situ Nuclear Magnetic Resonance probes to survey the field.

A similar equipment would be able to provide rather easily a momentum measurement with accuracy of 0.1 % or better at the LHC.

3.4 RF Frequency of Protons and Ions

This absolute momentum calibration method takes advantage of the fact that for a given LHC dipole field setting, the revolution frequency (respectively the speed) is different for ions and protons due to the different ratio of charge over rest mass. With this technique a precise energy calibration was performed at LEP with protons and positrons at 20 GeV/c [11]. Two such calibrations were performed at the SPS, one in 1991 using proton and Oxygen ions at 270 GeV/c [12] and another in 2002 using proton and Pb^{53+} beams at 450 GeV/c [13].

The speed βc of a particle is related to the revolution frequency f_{rev} and the RF frequency f_{RF} by

$$\beta c = C f_{rev} = \frac{C f_{RF}}{h} \tag{5}$$

where h is the harmonic number of the RF system (h = 35640 for the LHC). C is the machine circumference. To determine the speed β and therefore the particle momentum, both the machine circumference and the revolution (or RF) frequency must be known.

The trick to determine momentum and machine circumference at the same time is to measure the revolution frequency for two particles with charge over mass ratio that are injected into exactly the same magnetic machine and on the same orbits. The speed $\beta_p c$ of the proton beam is related to its momentum P and its rest mass m_p by the well known relation

$$\beta_p^2 = \frac{P^2}{P^2 + (m_p c)^2} \ . \tag{6}$$

An ion with charge Ze, injected into the same magnetic machine and on the same orbit than the proton beam has a momentum $P_i = ZP$. The speed $\beta_i c$ of the ions is

$$\beta_i^2 = \frac{P^2}{P^2 + (m_i c/Z)^2} \tag{7}$$

with m_i the ion rest mass. These two equations can be solved for the proton beam momentum P, yielding

$$P = m_p c \sqrt{\frac{\kappa^2 \mu^2 - 1}{1 - \kappa^2}} \tag{8}$$

with

$$\kappa = \beta_i / \beta_p = f^i_{RF} / f^p_{RF} \tag{9}$$

and

$$\mu = \frac{m_i}{Z m_p} \, . \tag{10}$$

μ is the number of nucleons per charge of the ion, μ = 2.517 for the fully stripped Pb^{82+} lead ions that are available at the LHC. Equation (8) can be approximated by

$$P \cong m_p c \sqrt{\frac{f^p_{RF}}{2 \Delta f_{RF}} (\mu^2 - 1)} \tag{11}$$

where $\Delta f_{RF} = f^p_{RF} - f^i_{RF}$ is the RF frequency difference between the proton and ion beams.

The measurement error on P is dominated by the accuracy of the RF frequency determination since all other parameters entering Equations (8) and (11) are known with high accuracy. The measurement error σ_P on P is dominated by the term

$$\frac{\sigma_P}{P} \simeq \frac{\sqrt{\sigma^2_{f^p_{RF}} + \sigma^2_{f^i_{RF}}}}{2 \, \Delta f_{RF}} \tag{12}$$

with $\sigma_{f^p_{RF}}$ and $\sigma_{f^i_{RF}}$ the measurement errors on the RF frequencies of the proton and ion beams.

The frequency difference Δf_{RF} between the beams follows from Equation (11),

$$\Delta f_{RF} \cong \left(\frac{m_p c}{P} \right)^2 \frac{f^p_{RF}}{2} (\mu^2 - 1) \tag{13}$$

and scales quadratically with μ. The dependence on $1/P^2$ makes the measurement very difficult at the highest energies when the speeds of both beams approach c and the speed difference vanishes.

The frequency difference Δf_{RF} is shown as a function of the LHC proton momentum P in Figure 1. The frequency difference shrinks by more than 2 orders of magnitude between 450 GeV/c and 7 TeV/c. Frequency difference values as well as the sensitivity with respect to energy changes $d(\Delta f_{RF})/dP$ are given for some LHC energies in Table 1. For a momentum determination at 7 TeV/c with a relative accuracy of 10^{-3}, the frequency difference must be determined with an error not exceeding 40 mHz, which corresponds to an accuracy on the machine radius of ≤ 0.4 μm.

3.4.1 Measurement Challenges

An accurate calibration at the level of 0.1−1% at 3.5−7 TeV/c requires a measurement of the radial offset between proton and lead beams at the level of 1−10 μm (Table 1). This is quite a challenge since the LHC ring is not stable to this level on the time scale of a few hours.

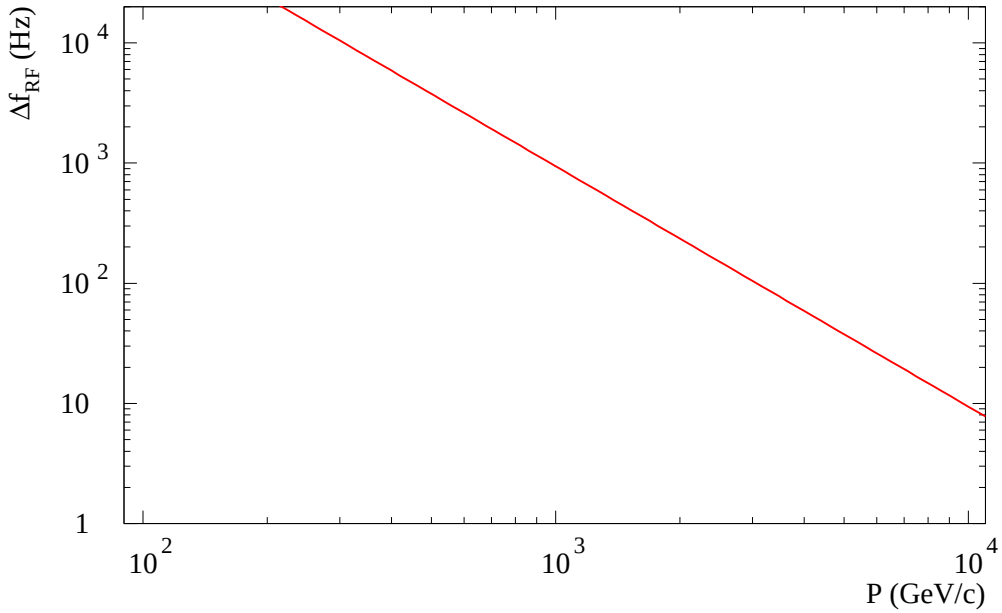

Figure 1: Expected central RF frequency difference between proton and Pb^{82+} beams as a function of the beam momentum at the LHC.

Momentum P (GeV/c)	Δf_{RF} (Hz)	$d(\Delta f_{RF})/dP$ (Hz/GeV)	$\sigma_{\Delta f}$ (Hz)	σ_R (μm)
450	4650	-20.7	9.1	96
3500	76.87	-0.044	0.15	1.6
4000	58.85	-0.029	0.12	1.3
6500	22.99	-0.0071	0.046	0.49
7000	19.22	-0.0055	0.039	0.41

Table 1: This table presents a list of variables that are of interest for a few relevant proton momentum values (P, left column). The second column from the left corresponds to the RF frequency difference Δf_{RF} between a proton and a Pb^{82+} beam. The third column from the right gives the sensitivity of Δf_{RF} to the momentum, $d(\Delta f_{RF})/dP$. The fourth and fifth column give the accuracy $\sigma_{\Delta f}$ on Δf_{RF} and σ_R on the mean machine radius required to reach a 0.1% accuracy for the energy measurement.

Geological movements like Earth tides may change the circumference by up to 1 mm with 12 hours [14]. Due to the limited accuracy of the tidal prediction (at level of a few percent) and to the presence of other slow ground movements [15], it is not possible to accurately predict changes to C_c to better than ≈ 0.1 mm. A direct measurement of the radial position of the beams is necessary, requiring well calibrated beam position monitors (BPMs) or more complicated measurement techniques [16].

It is very difficult to perform accurate measurements as long as the proton and lead beams are injected and ramped in separate machine cycles as it was done up to 2011, with either proton-proton or lead-lead runs. In such conditions measurements on protons and lead ion beams require separate machine cycles spaced by at best a few hours. Attempts to calibrate the momentum with separate proton and lead cycles yielded uncertainties at the level of 100 GeV/c at 3.5 TeV [7].

The situation changed significantly in 2013 with the mixed proton-lead run, where both particle types are present at the same time in the LHC, albeit in separate rings. The frequency offsets can be measured at the same time for protons and ions, cancelling out effects from geological deformations of the tunnel and from certain BPM errors.

4 Mixed Operation with Proton and Lead Ion Beams

The mixed operation mode with protons circulating in LHC ring 1 and lead beams in LHC ring 2 (and vice-versa) was first demonstrated in 2011 [4]. First collisions were delivered in this mode at 4 TeV in September 2012 [5]. In a 4 week run that took place between January and mid-February 2013, over 30 nb^{-1} of integrated luminosity were delivered to each of the experiments. The data used for the beam energy measurement was collected parasitically during this 4 week period. Roughly one half of the run was operated with protons in ring 1 and lead in ring 2, and the other half in the reverse configuration with protons in ring 2 and lead in ring 1.

Operation mixing proton and ions requires special RF settings and manipulations. The operational cycle in this mode can be broken up into the following phases.

1. **Injection**: The beams are injected one after another at 450 GeV, starting with the protons (IBS is stronger for lead ions). The RF systems of the beams are unlocked: the RF frequencies of the beams are differ typically by 4650 Hz and can be adjusted independently. The beams are not synchronous at the collision points due to the frequency difference.
2. **Ramp**: During the energy ramp from 450 GeV to 4 TeV the RF systems remain unlocked. The frequency of each beam follows the evolution of the beam energy to maintain the beams centered in the vacuum chambers. As the energy increases the RF frequency of the two rings approach to within 58 Hz (Figure 2).
3. **RF manipulations at flat top**: On the 4 TeV flat top the RF frequencies of the two beams are forced to a common frequency (typically the average frequency of protons and lead ions), and the beams are re-synchronized to ensure that the bunches collide at the experimental interaction points. After the RF manipulations, the two beams move off-center since the common frequency does not match the frequency required to center the beams in the quadrupoles.
4. **Squeeze**: Once the beams are synchronized, the optics at the interaction points is changed to reduce the betatron function at the collision point (β^*) and enhance the luminosity. The duration of the squeeze phase is approximately 15 minutes.
5. **Collisions**: Finally the beams are brought into collision ('stable beams') in the experimental interaction regions to deliver collisions for the experiments.

The evolution of the RF frequency in the ramp and on the flat top is shown in Figure 2.

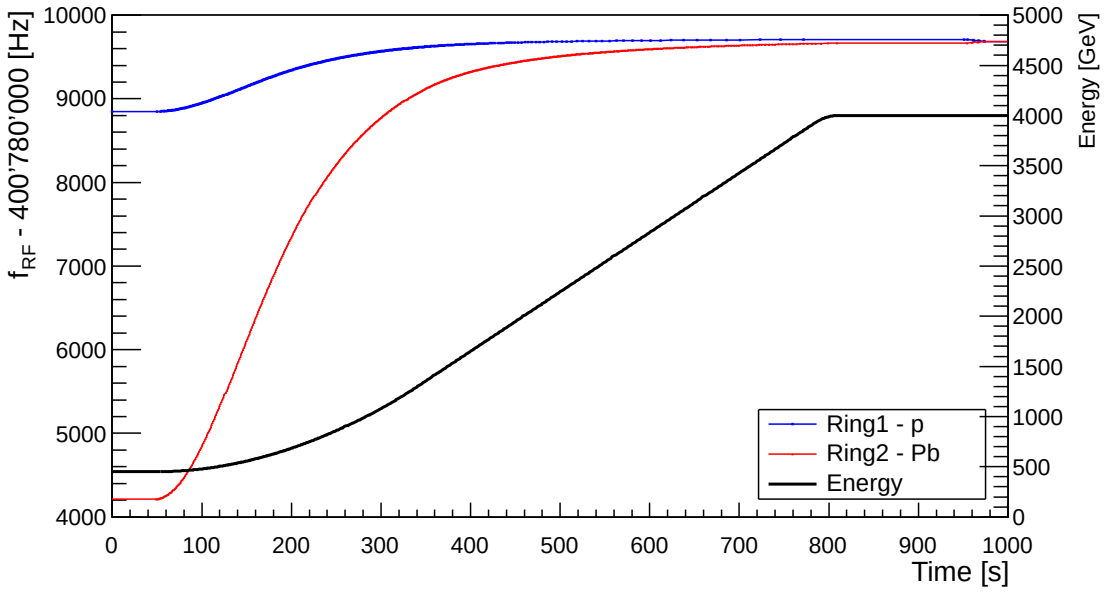

Figure 2: Evolution of the proton and lead ion RF frequencies during the ramp. The frequencies are locked together at 4 TeV (around time 960).

5 Frequency Offset Measurements

The determination of the beam energy is based on the radial offset of the orbits at the end of the RF manipulations at 4 TeV (phase 3 of Section 4). The beams are forced on a common frequency that is on average 29 Hz too low for the protons and 29 Hz too high for the lead ions. As a consequence the proton beam moves radially outward while the lead beam moves radially inward. To determine the beam energy, the radial offsets measured by the BPMs are converted into equivalent RF frequency shifts. Figure 3 shows the orbit shift of the two beams when they are forced to the common frequency during the RF manipulation. The typical mean radial change is 0.3 mm for each beam, a frequency change of 1 Hz shifts the beam radially by 10.6 μm. Systematic errors on the radial position determination due to BPM scale and offset errors are the limiting factor for the measurement accuracy and must be well controlled.

The relative momentum offset of the beam due to its radial shift in the ring can be estimated from the BPM readings in the horizontal (bending) plane using the following Equation,

$$\frac{\Delta P}{P} = \frac{\sum_{i=1}^{N} D_{x,i} x_i}{\sum_{i=1}^{N} D_{x,i}^2} \tag{14}$$

where i labels the BPMs and N is the total number of BPMs. $D_{x,i}$ is the horizontal dispersion at the BPM with index i and x_i is the measured horizontal beam position at the same BPM. The momentum offset is converted into a RF frequency offset through the momentum compaction

Figure 3: Beam position change for the protons in ring 1 (top) and lead ions in ring 2 (bottom) between start and end of the RF manipulations at 4 TeV. For both plots the horizontal axis represents the BPM index, while the vertical axis is the horizontal (radial) beam position measured at each BPM in mm. The position shift is modulated by the horizontal dispersion $D_{x,i}$ at each BPM.

factor α_c,

$$\Delta f_{RF} = -\frac{f_{RF}}{\alpha_c}\frac{\Delta P}{P} = -\frac{f_{RF}}{\alpha_c}\frac{\sum_{i=1}^{N} D_{x,i}x_i}{\sum_{i=1}^{N} D_{x,i}^2} \tag{15}$$

The main issue for the accuracy of the measurements of the frequency offset is coming from possible systematic offsets between the center of the BPMs and the center of the quadrupoles. A mean systematic alignment offset will lead to an error on the reconstructed frequency offset, limiting the accuracy when a single configuration with protons in ring 1 and lead ions in ring 2 is used (for example). For a constant measurement offset of the BPMs, it is possible to cancel the systematic error by inverting the beams in the rings, i.e. by measuring in the configuration

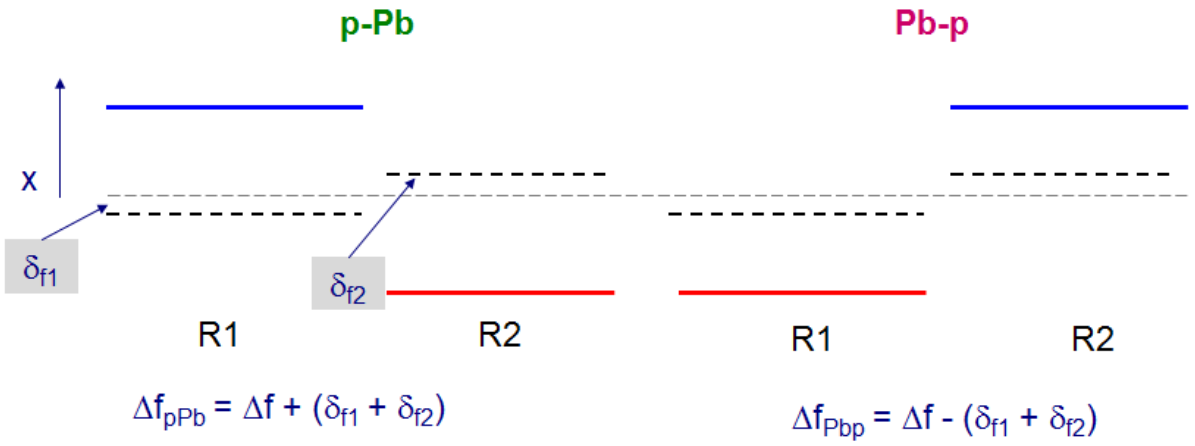

Figure 4: Principle of the cancellation of systematic errors on the radial position by inversion of the protons and lead ions in the two rings.

with protons in ring 1 and lead ions in ring 2 (**p-Pb**) as well as in the reverse configuration with with protons in ring 2 and lead ions in ring 1 (**Pb-p**).

If δ_{f1} (δ_{f2}) is the systematic frequency error that is introduced by a center offset of the BPMs in ring 1 (ring 2), see Figure 4, the measured frequency difference Δf_{pPb} between proton and lead in p-Pb configuration is given by

$$\Delta f_{pPb} = \Delta f_{RF} + (\delta_{f1} + \delta_{f2}) \ , \tag{16}$$

while in Pb-p configuration the measurement yields

$$\Delta f_{Pbp} = \Delta f_{RF} - (\delta_{f1} + \delta_{f2}) \ . \tag{17}$$

Δf_{RF} represents the true frequency offset between protons and lead ions. It is assumed that the BPMs are only sensitive to the beam charge and do not change their characteristics when the beams are inverted. The real frequency is obtained by averaging the measurements taken in the two configurations since the systematic errors have exactly the opposite sign,

$$\Delta f_{RF} = \frac{1}{2}(\Delta f_{pPb} + \Delta f_{Pbp}) \ . \tag{18}$$

The potential of removing or at least reducing drastically the systematic error from center offsets of BPMs and quadrupoles makes the mixed mode with proton and lead ions very attractive for the energy measurement.

In the following sections and figures the following standard colour code is used for the data:

- Data points corresponding to operation in **p-Pb** mode are displayed in **green** colour.
- Data points corresponding to operation in **Pb-p** mode are displayed in **magenta** colour.
- Data points corresponding to **ring 1** are displayed in **blue** colour.
- Data points corresponding to **ring 2** are displayed in **red** colour.

5.1 Beam Position Monitor Calibration

Since the frequency shifts are obtained from the radial beam position as measured by the BPMs, the calibration of the BPM scale is critical to obtain accurate measurements.

The scale correction was determined with controlled RF frequency trims of 10 Hz over a range of ± 40 Hz around the central orbit. The calibrations were performed in fills 3499, 3500 and 3514, see for example Figure 5. Unfortunately the calibrations could not be repeated in later fills because of beam loss issues with the lead beam (due to large transverse emittances). In all cases the response of the BPMs was perfectly linear. For ring 1 all calibrations consistently yield a factor of $C_1 = 1.020 \pm 0.001$, for ring 2 the spread is somewhat larger with a calibration factor $C_2 = 1.023 \pm 0.003$. $C_{1(2)}$ are the scale corrections to be applied to the BPM data, they correspond to the ratio of frequency change reconstructed by the BPMs with respect to the true frequency change.

The scale factor can be checked with the radial position shift of each beam before and after the RF manipulation (phase 3 in Section 4), since the RF frequency change due to the RF manipulation is precisely measured. The orbit measurements are taken one second after arriving at the 4 TeV flat top, and one second after the start of the optics squeeze (to ensure a consistent treatment of the data for all fills). Due to the time interval between those two orbits, the frequency change must be corrected for tides. The tide corrections range between -2 and $+2$ Hz, the typical correction is however around 0.4 Hz. The ratio between the reconstructed RF frequency change (from the BPMs) and the measured frequency provides a verification of the BPM scale. The distribution of calibration factors is shown in Figure 6. The central values agree very well with the dedicated calibrations done with RF frequency steps. The calibration factor spread is relatively large due to the small frequency changes and to the time between the

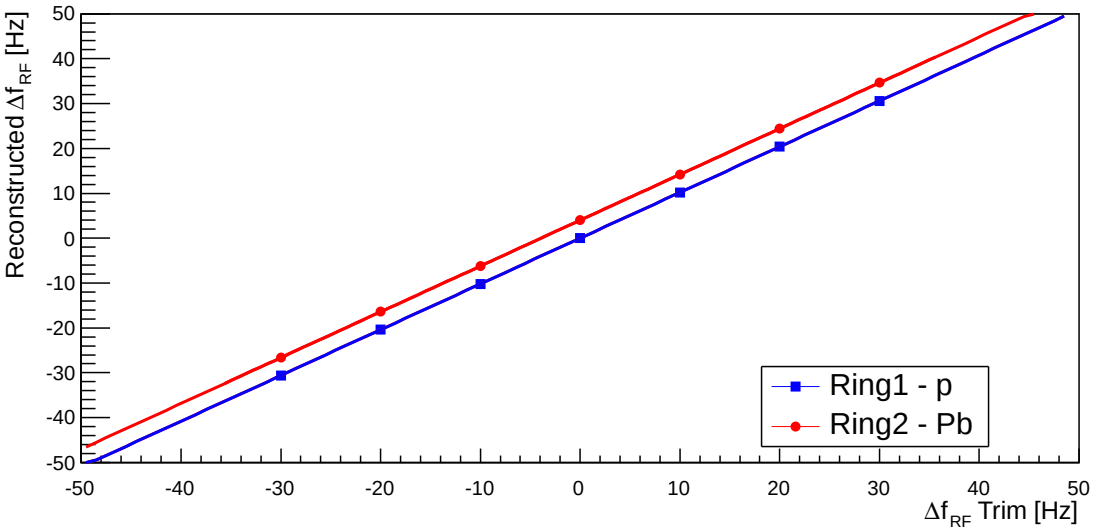

Figure 5: Calibration of the BPM scale with RF frequency trims (horizontal axis) in fill 3500 at 4 TeV before the RF manipulations. The vertical axis corresponds to the RF frequency value reconstructed from the BPMs. The beam 2 data points have been offset vertically by 4 Hz for clarity. The deviations from the data points to the straight lines are smaller than 0.1 Hz.

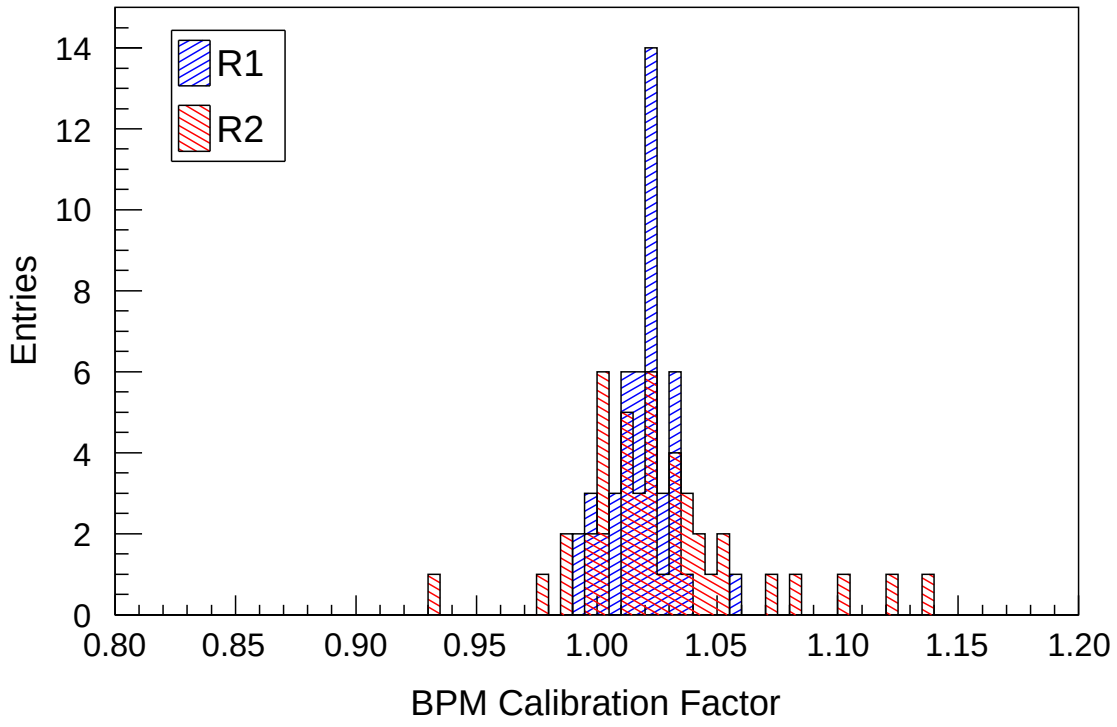

Figure 6: Distribution of the BPM calibration factors obtained from the orbit change during the RF manipulation at 4 TeV.

acquired orbits. While the spread for ring 1 is around 1% and is consisted with estimates based on the orbit accuracy, the spread of the calibration factors is significantly larger for ring 2. The same difference is also observed for the dedicated calibrations. The reason for the difference between ring 1 and ring 2 is not understood.

5.2 Horizontal Dispersion

Due to tidal deformations and other geological effects [14, 15], as well as manual trims of the RF frequency to adjust the beams (for example for losses), the radial position of the beams at the start of the squeeze at 4 TeV is modulated from fill to fill. The correlation between the reconstructed RF frequency offsets of the proton and lead beams at 4 TeV after RF manipulation is shown in Figure 7. There is a strong correlation between rings as expected for changes that shift the mean frequency or the machine circumference. The fill to fill shifts of the frequency offset can be used to reconstruct the horizontal dispersion of the two rings (assuming that the BPM offsets are stable). The reconstructed dispersion, which includes the BPM scale correction, is compared to the model dispersion in Figure 8. The agreement is excellent, within the known 10% beta-beating. This results also indicates that the response of all the BPMs that are considered for the measurement is correct.

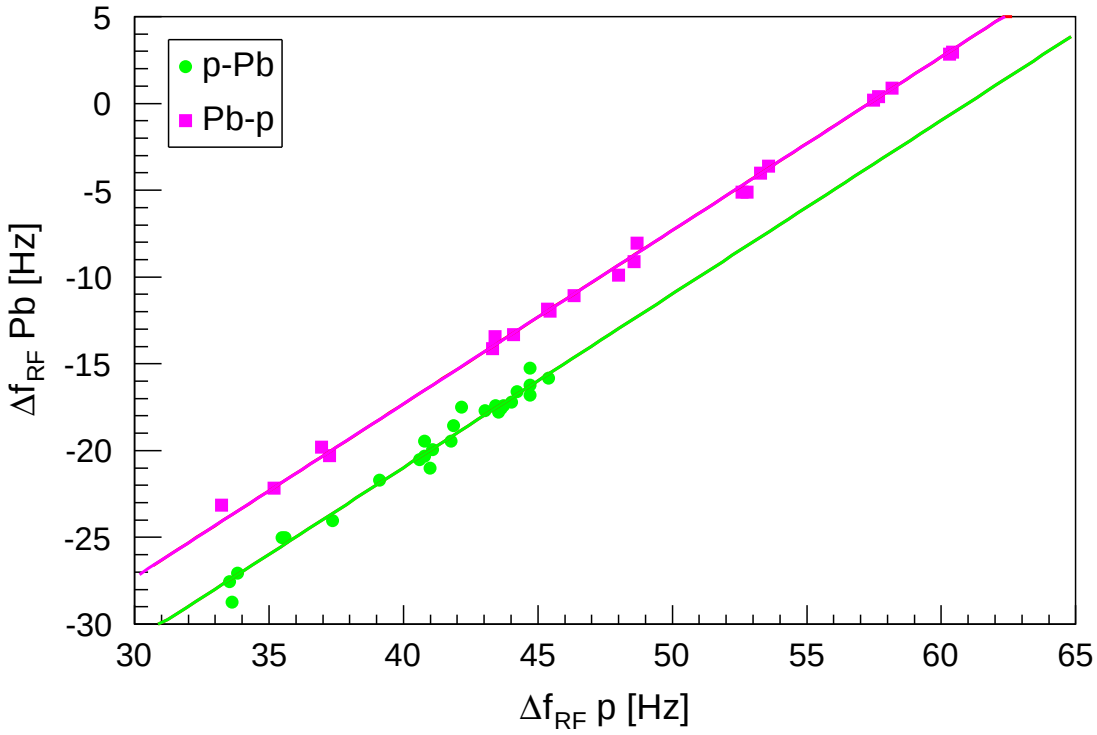

Figure 7: Reconstructed RF frequency shifts of the proton (horizontal axis) and lead (vertical axis) beams in p-Pb and Pb-p mode. The vertical offset between the two data point groups (lines) is due to the systematic errors δ_{f1} and δ_{f2} as quoted in Equations (16) and (17).

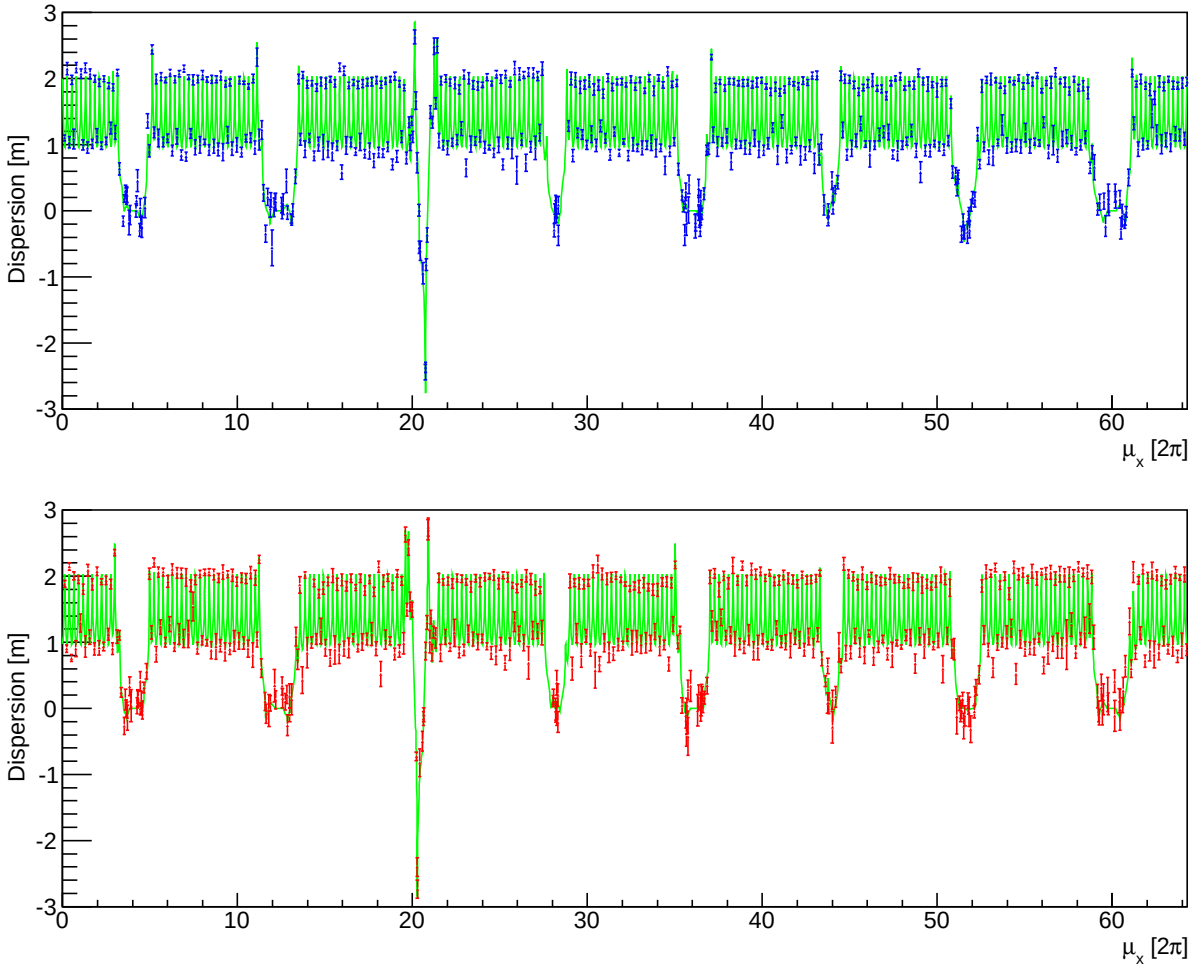

Figure 8: Reconstructed dispersion of ring 1 (top, blue points) and ring 2 (bottom, red points) and model dispersion (green).

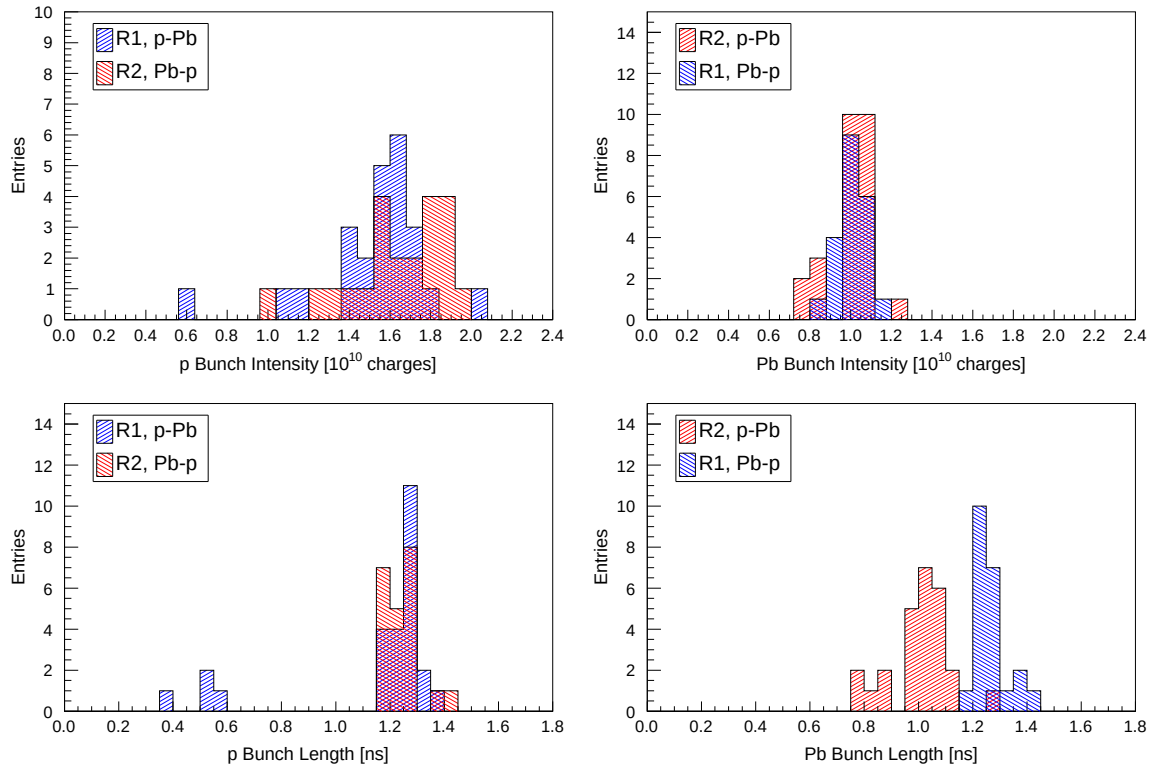

Figure 9: Parameters of the proton and lead bunches during the p-Pb and Pb-p phases: bunch intensity (top) and bunch length (bottom).

5.3 Beam Conditions

The distribution of the bunch intensities that were used for the orbit measurements is shown for both proton and lead beams and both modes in Figure 9. With the exception of a few setup fills where the intensity was below 10^{10} charges, the proton bunch intensity was $> 10^{10}$ charges, with a mean of $\approx 1.6 \times 10^{10}$ charges. The average lead bunch charge was lower, at $\approx 10^{10}$ charges, the lowest bunch charge was around 0.7×10^{10} charges.

The distribution of bunch lengths (4σ) is also given in Figure 9. Even though no measurable influence of the bunch length could be observed in a dedicated test, a change of bunch length could potentially have a small influence on the BPM measurements and change the dependence on intensity as the peak charge density is affected in the longitudinal plane. For protons the bunch length was around 1.2 ns for all but the setup fills. For lead bunches there is a larger spread and a difference between the two modes because the length was adjusted to improve lifetimes and emittance growth from Intrabeam Scattering (IBS) during the Pb-p period.

5.4 Bunch Current Dependance

The bunch current is important because of the known dependance of the BPM electronics accuracy on this beam parameter. The sensitivity is due to the principle of the Wide Band Time Normalization electronics and it is in principle well understood [17].

To assess the importance of this sensitivity on the measurement of the radial orbits and

reconstructed frequencies, bunches were scraped on collimators at injection during stable conditions. The apparent change of the radial orbit position due to intensity systematics can be assessed during such tests. The results are shown in Figure 10 for ring 1 and ring 2. While for ring 1 the radial position measurement is stable down to $\approx 6 \times 10^9$ charges, the situation is less favorable for ring 2 where systematic effects become visible around $\approx 10^{10}$ charges. This difference is explained by the presence of (unused) intensity measurement electronics in the ring 1 acquisition chain, affecting the systematic electronics effects.

While this systematic effect does not impact the measurement of the protons due to the higher bunch charge, the lead ion bunch measurements in p-Pb configuration with lead in ring 2 are in a region where the systematic errors may reach 0.5 Hz according to the scraping tests. This will be considered later in the analysis.

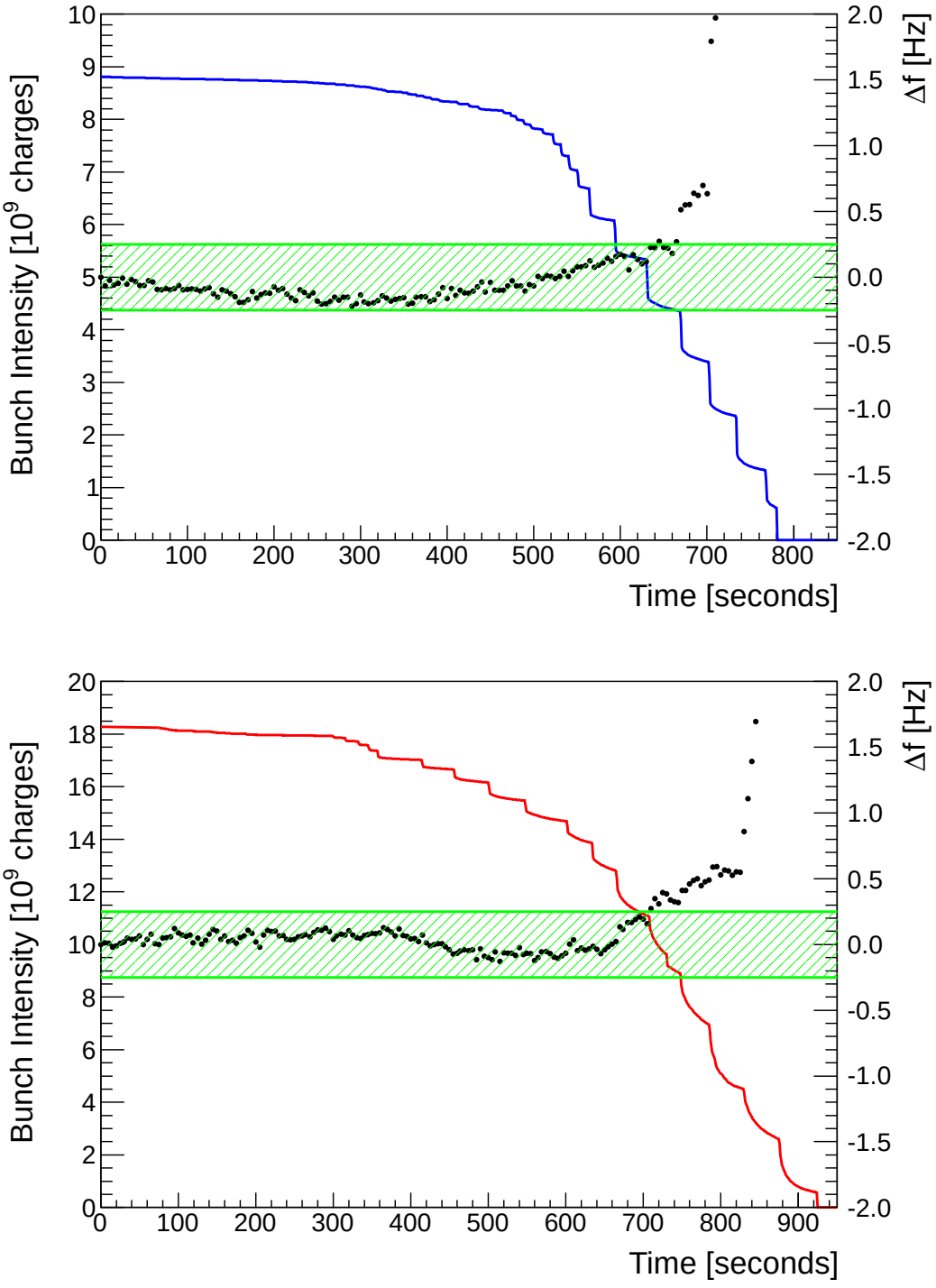

Figure 10: Apparent change of the radial beam position (black points), converted into RF frequency change, as a function of the bunch intensity of ring 1 (blue trace, top) and ring 2 (red trace, bottom). The bunch intensity was scraped on a collimator over a short time interval. The green band corresponds to a frequency range of ± 0.25 Hz.

6 Energy Measurement at 4 TeV

The frequency difference between protons and lead ions is extracted from orbits acquired at a standard time corresponding to the start of the optics squeeze (Section 4). For each beam the frequency offset with respect to the center of the BPMs is determined using Equation (15). The reconstructed frequencies are corrected for the average BPM scale calibration factors given in Section 5.1, and the difference in frequency between protons and lead ions is obtained by subtracting the frequency offsets of the two beams with the correct sign convention.

To evaluate systematic effects the data was analysed using different cuts and sub-samples of the BPMs. Three different samples were considered:

- BPM sample **Sa**: this is the *standard* sample based on BPMs with dispersion larger than 1 m. The number of good BPMs in this sample is 390 for ring 1 and 389 for ring 2.
- BPM sample **Sb**: only BPMs in the LHC arcs with dispersion larger than 1.5 m were used to extract the frequency offsets. This essentially halves the number of BPMs and biases toward BPMs with higher sensitivity to frequency offsets.
- BPM sample **Sc**: the standard cut on the dispersion of 1 m was used, but only BPMs in half of the machine were considered, between phase advance of $36 \times 2\pi$ and $4 \times 2\pi$, see Figure 8. This corresponds to the ring section from CMS to ATLAS in the direction of beam 1.

The following standard cuts were also applied to minimize systematic errors:

- The bunch intensity of the proton bunches must be $\geq 1.1 \times 10^{10}$ charges.
- The bunch intensity of the lead ion bunches must be $\geq 0.8 \times 10^{10}$ charges.
- The bunch length of the proton bunches must be ≥ 1 ns.
- The bunch length of the lead bunches must be ≥ 0.95 ns
- The calibration factor derived during the RF manipulation must be in the range 0.97 to 1.07 (Figure 6).

The complete measurement sample consists of 26 fills in p-Pb mode and 22 fills in Pb-p mode. After applying the cuts on intensity, bunch length and calibration factors, the number of fills is reduced to 18 in p-Pb mode and to 20 in Pb-p mode. The resulting frequency difference Δf_{RF}, obtained from BPM sample **Sa**, is shown for the remaining 38 fills in Figure 11. On Figure 11 a small time dependance of the result is possibly present, with a slope of around 0.6 Hz in each period. This trend is also present if the analysis is repeated for the other BPM samples. The offset of ≈ 4 Hz between the data of the two modes reflects the systematic error on the frequency offset described in Section 5. This corresponds to a radial offset between average center of BPMs and quadrupoles of $\simeq 20$ μm. To obtain an accurate result the data of the two periods must be averaged.

The possible time trend in the data of Figure 11 may have a variety of origins, including measurement fluctuations. A real change of energy seems excluded because the tune settings were very stable in the entire period. Orbit effects are not very likely since the r.m.s. change of the orbit between fills is in the range of $40-50$ μm (after subtraction of the contribution from the frequency offset) and shows no trend. A change of the BPM offsets by ≈ 5 μm or of the BPM calibration by $\approx 1\%$ could explain the effect.

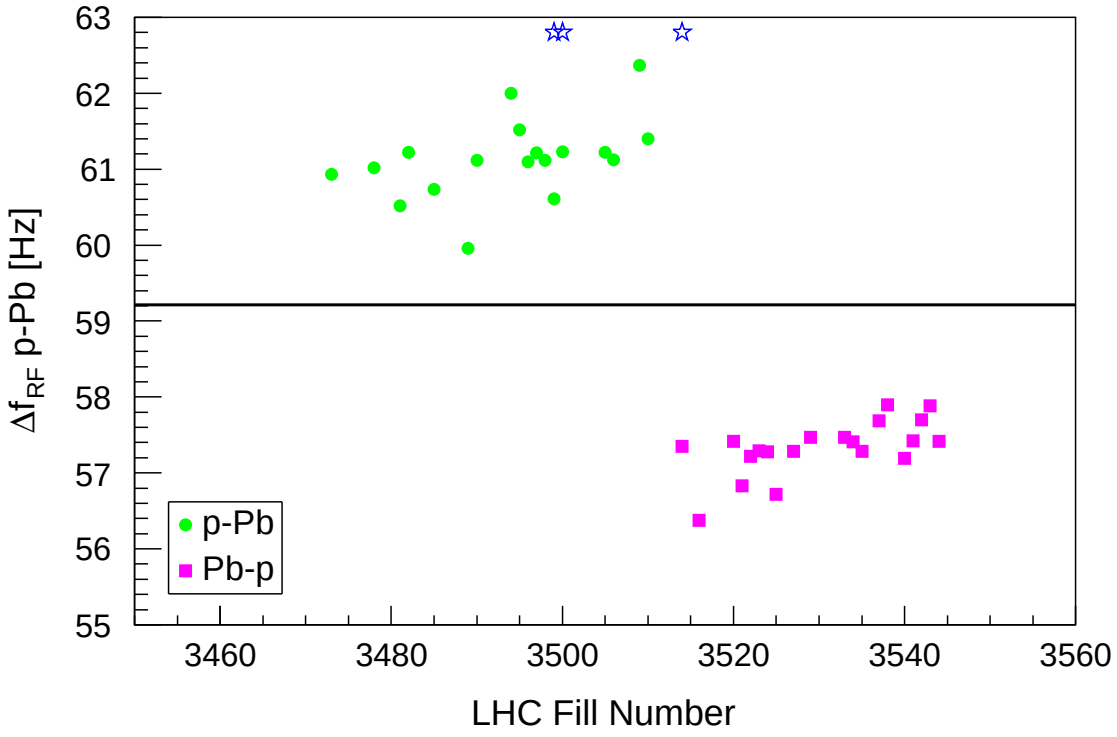

Figure 11: Time dependence of the frequency differences of proton and lead beams (as a function of the LHC fill number). The symbol ($\star$) indicates BPM calibrations.

The distribution of Δf_{RF} values is shown in Figure 12 with two different cuts on the data sets. The top plot of Figure 12 includes all 38 fills with standard cuts. For the bottom plot an additional cut on the fill number was applied: only the 10 fills around the moment when protons and lead ions were reversed were retained. This sub-sample is also recorded close to the BPM scale calibrations. Based on the r.m.s. orbit changes of $40-50$ μm one expects a spread of the Δf_{RF} values for each period of ≈ 0.35 Hz. The observed spreads are somewhat larger, in the range of 0.35 to 0.52 Hz. But for the sub-sample of 10 fills the spread is consistent with the expected spread.

The results for Δf_{RF} averaged over the two periods for different samples and cuts are shown in Table 2. Besides varying the BPM sample (sets 4 and 5) and the fill selection (sets 2 and 3) as described above, the analysis was also repeated for orbit acquired at the start of the stable beams period (i.e. with beams in collision, set no. 5). The orbits in stable beams are typically acquired 20 minutes after the start of the squeeze, this gives an estimate of possible systematic effects from the BPM electronics temperature. There are also fewer fills, since some fills were dumped in the squeeze or used for beam setup. The results are stable with respect to the cuts, all differences are consistent with statistical fluctuations.

Data set no. 2 is used as reference for the energy determination as it is likely to have the smallest bias and systematic error. Those fills are close in time to the calibration fills. From Table 2 a systematic error of ± 0.25 Hz is assigned to the choice of the BPM selection. Since the lead ions bunch intensities lie in a range where BPM systematic error start to kick in, a additional

Set	Δf_{RF} (Hz)	Data sample and cuts
1	59.24 ± 0.15	BPM sample **Sa**, standard cuts
2	59.21 ± 0.17	BPM sample **Sa**, standard cuts, 10 fills per period (3495-3530)
3	59.15 ± 0.13	BPM sample **Sa**, no cuts (all fills)
4	59.24 ± 0.14	BPM sample **Sb**, standard cuts
5	59.49 ± 0.18	BPM sample **Sc**, standard cuts
6	59.51 ± 0.12	BPM sample **Sa**, orbits are acquired in stable beams, standard cuts

Table 2: Results for the frequency differences of proton and lead beams Δf_{RF} for different analysis cuts. The errors on the frequency are statistical only. It must be noted that the statistical errors are strongly correlated.

Contribution	Syst. Error (Hz)
BPM selection	0.25
Bunch intensity effect on BPM measurements	0.25
Average BPM scale uncertainty of 0.5%	0.30
Drift of the frequency difference	0.60
Total	0.76

Table 3: Contributions to the systematic error on the proton lead frequency difference Δf_{RF}.

systematic error of $\pm$0.25 Hz was assigned to this effect. The uncertainties on the BPM scale directly affect the result. A systematic error of 0.5% is assigned to the scale calibration, which results in a $\pm$0.3 Hz systematic error on the frequency. Finally a $\pm$0.6 Hz systematic uncertainty is added to account for the possible (and unexplained) drift in the data visible in Figure 11. The total systematic error is obtained from the quadratic sum of the 4 contributions (assumed to be largely independent), yielding a final error of $\pm$0.76 Hz. All contributions are summarized in Table 3. The result for the frequency difference between protons and lead ions at 4 TeV is

$$\Delta f_{RF,4TeV} = 59.21 \pm 0.15 \text{ (stat)} \pm 0.76 \text{ (syst) Hz} . \tag{19}$$

This result can be converted into a beam momentum at 4 TeV with the constants given in the Appendix

$$P_{4\text{TeV}} = 3988 \pm 5 \text{ (stat)} \pm 26 \text{ (syst) GeV/c} = 3988 \pm 26 \text{ GeV/c} \tag{20}$$

where the total error is obtained from the quadratic sum of the statistical and of the systematic error. If only the three fills with BPM calibration are used to determine the energy, the frequency offset is

$$\Delta f_{RF,4TeV} = 59.13 \pm 0.43 \text{ (stat) Hz} \tag{21}$$

The statistical error is based on a assumed measurement spread of 0.35 Hz as expected for the fill-to-fill r.m.s. orbit change, which also matches rather well the observed width (Figure 12). The value obtained from those 3 calibrated fills is in good agreement with Equation (19).

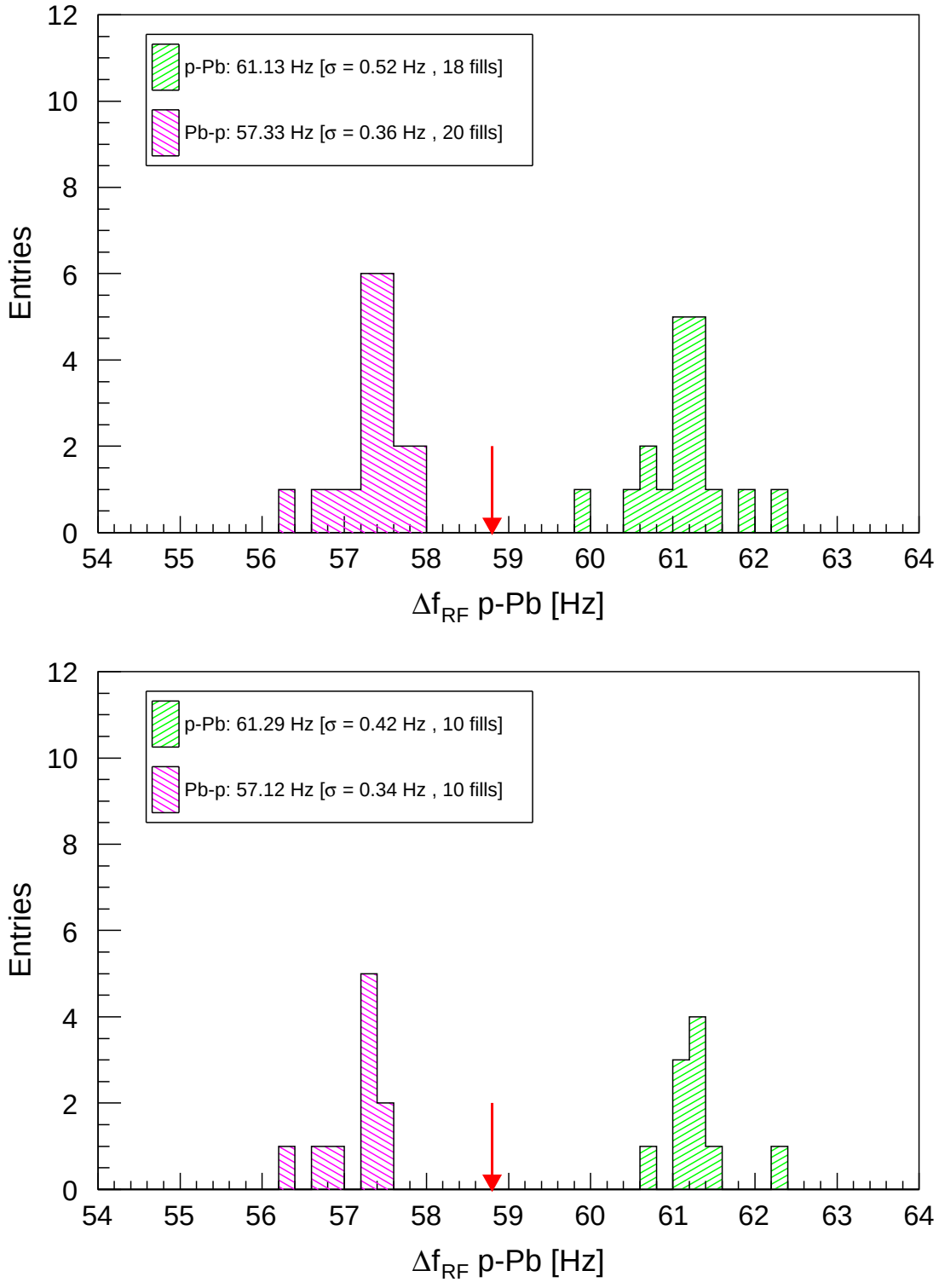

Figure 12: Distribution of frequency differences Δf_{RF} of proton and lead beams. The arrow corresponds to the expected value for an energy of 4 TeV. The top figure corresponds to Set 1 and the bottom figure to Set 2 of Table 2.

7 Energy Measurement at Injection

The energy measurement was repeated at injection with orbits acquired just before starting the ramp to 4 TeV. At that moment of the cycle the RF systems of the two rings are still uncoupled (Section 4). The beams are operated with a large RF frequency difference. The frequency offset between protons and lead ions is obtained from the recorded RF frequencies for each ring, corrected for the radial offset measured by the BPMs based on BPM sample **Sa**. In general the beams are well centered in this phase, and the corrections from the orbit measurements are small (between -27 and $+3$ Hz) compared to the total frequency difference of 4.6 kHz. For this reason the BPM scale calibration uncertainty does not affect the result for injection in a significant way.

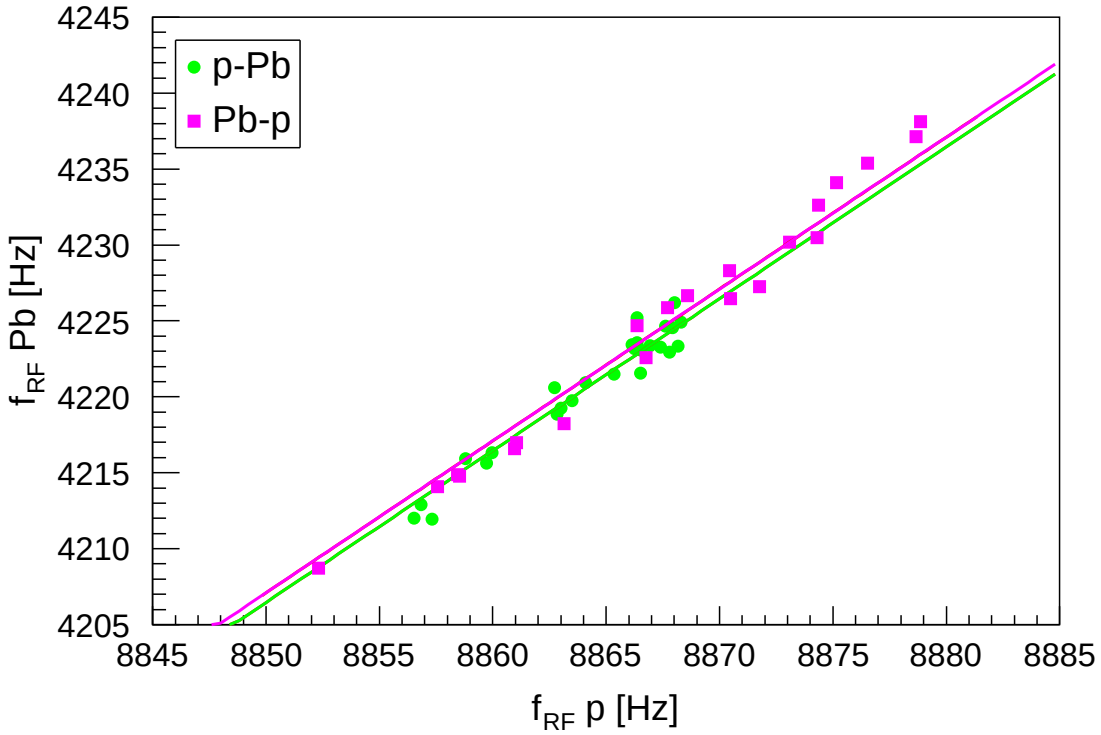

Figure 13: Reconstructed RF frequencies of the proton (horizontal axis) and lead (vertical axis) beams in p-Pb (green) and Pb-p (magenta) mode at injection. An offset of 400'780'000 Hz has been subtracted from the RF frequency values presented in this figure.

Figure 13 shows the correlation between the proton and lead ion RF frequencies. The offset between the 2 periods is smaller than at 4 TeV. Figure 14 gives the evolution as a function of the fill number and the histogram of the reconstructed frequency differences at 450 GeV. The step that is visible in the top plot in Pb-p mode occurs at fill number 3534 and is due to a change of the integrated field of the horizontal orbit correctors. This change was applied to adjust the momentum matching between SPS and LHC. The relative change in field is 2.4×10^{-4} for ring 1 and 2×10^{-4} for ring 2, corresponding to an average momentum change $\Delta P = 0.099$ GeV. This change reduces Δf_{RF} by 2.05 Hz, in good agreement with the step in the data.

To avoid introducing corrections for the orbit corrector changes, fills after number 3533 have been excluded in the analysis and do not appear in the lower plot of Figure 14. In the p-Pb period only the last 10 fills were retained (see 4 TeV case). Contrary to the situation at 4 TeV, the offset of the measurements between the p-Pb ad Pb-p periods is small. This difference can be explained by the absolute orbit at injection which differs from the orbit at 4 TeV. In addition the corrector settings are not identical which also influences the mean position of the beams in the BPMs of the two rings. In the p-Pb period the evolution of Δf_{RF} exhibits a drift of ≈ 2 Hz. In each period the orbits and corrector settings were stable (excluding the change due to energy matching). The r.m.s. orbit stability was ≈ 50 μm after subtraction of the frequency offsets, showing no particular systematic effect. The orbit stability is consistent with the typical fill-to-fill reproducibility. The expected spread of Δf_{RF} is around 0.35 Hz for each period, while the observed spreads are slightly larger than 0.5 Hz. No significant shift of the mean vertical position is visible which would be a possible indication of bias from BPM electronics temperature.

Assuming conservatively a total systematic error of ± 2 Hz on the averaged frequency difference, the result for the frequency difference between protons and lead ions at 450 GeV is

$$\Delta f_{RF,inj} = 4644.2 \pm 0.2\ (\mathrm{stat})\ \pm 2.0\ (\mathrm{syst})\ \mathrm{Hz} \tag{22}$$

This result can be converted into a beam momentum at injection of

$$P_{\mathrm{inj}} = 450.28 \pm 0.01\ (\mathrm{stat})\ \pm 0.11\ (\mathrm{syst})\ \mathrm{GeV/c} \tag{23}$$

A contribution to the systematic error from the orbit corrector magnets of 0.05 GeV was added in quadrature to the uncertainty arising from the frequency difference. Contrary to the case of 4 TeV this contribution is not negligible at injection due to the much smaller relative uncertainty on the beam energy.

This result for the momentum at injection is in excellent agreement with previous measurements [7]. A cross calibration of the LHC injection momentum with the SPS momentum at extraction through a measurement of the momentum offset of the beam injected into the LHC yields

$$P_{\mathrm{inj}} = 450.25 \pm 0.25\ (\mathrm{syst})\ \mathrm{GeV/c} \tag{24}$$

The SPS flat top field was calibrated in 2002 in a similar way with lead ion beams [13].

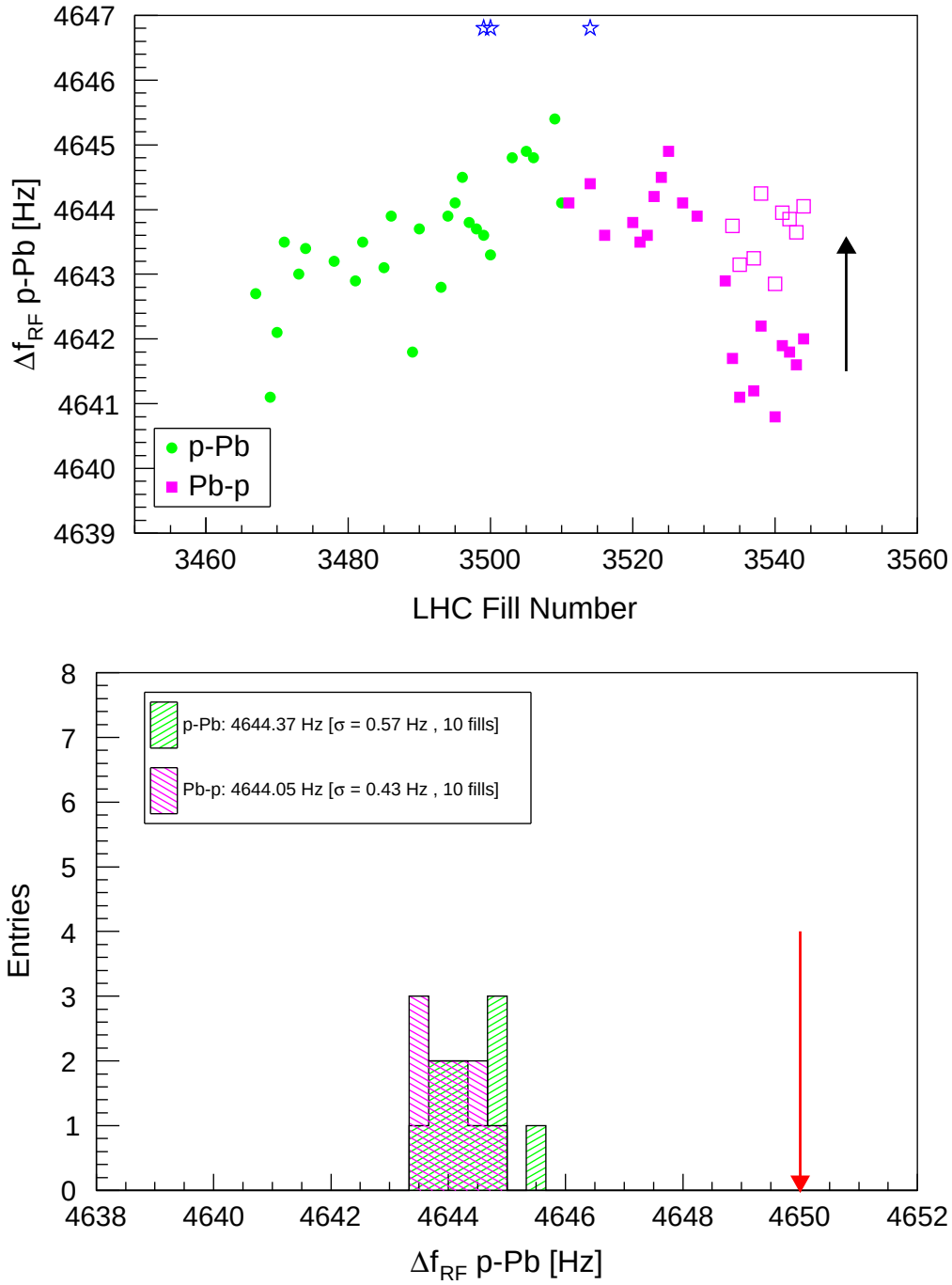

Figure 14: Top: Time dependence of the frequency difference Δf_{RF} of protons and lead ions (as a function of the LHC fill number). The jump in the values after fill 3533 (Pb-p period) is due to a change in the horizontal corrector settings. The corrected data is indicated by the symbol □ . The arrow indicates the size of the correction. The symbol ($\star$) indicates BPM calibrations. Bottom: Histogram of Δf_{RF}, the arrow corresponds to the expected value for an energy of 450 GeV. The values corresponding to the period after the jump at fill 3534 have been excluded, the fills are the same than for the 4 TeV analysis.

8 Time Dependence of the Energy

The energy of the LHC beams may vary with time due to changes of the dipole field, changes of the orbit corrector settings and geological effects that influence the circumference.

The stability of the LHC dipole field at 4 TeV can only be assessed indirectly since no continuous measurement is available. The data collected during the p-Pb run only indicates that the energy stability is better than 1%. The reproducibility of the LHC machine transverse tunes over time during the pp run is at the level of $\delta Q \approx 0.02$ or better. For a total integer tunes of 64 (horizontal plane) and 59 (vertical plane), this yields a dipole field stability of better than 3×10^{-4}. Such a good stability at high field is not surprising since the magnets

- are operated by definition at a stable temperature of 1.9 K,
- are cycled in a systematic way before each injection to ensure the highest possible machine reproducibility [18].

The horizontal orbit corrector magnets are used primarily to correct the closed orbit of the two beams, but when they are shifted systematically in one direction, their combined field can affect the beam energy [10]. At the LHC the horizontal correctors are used at injection to match the energy of each ring with the energy of the beam extracted from the SPS. Typical corrections are at the level of $\pm 3 \times 10^{-4}$, the differences between the rings never exceed 2×10^{-4}. This correction is only applied at injection and not propagated to high energy. The energy is re-adjusted typically 2 to 3 times per year. At high energy the relative correction due to correctors does not vary by more than $\pm 10^{-4}$.

The circumference of the LHC is oscillating periodically due to Earth tides. The total relative energy swing from the tides is 1.3×10^{-4} which corresponds to a RF frequency swing (to maintain the beam in the center) of 17 Hz. The circumference swing is 1.1 mm. An example is given for the LHC run in 2012 in Figure 15. The radial feedback loop corrects the tidal effects by adapting the frequency to center the beams. This loop is used during ramp and squeeze, it ensures that at the start of the stable beam periods the effect of the tides is essentially zeroed. Tidal effects that occur during the stable beams period are corrected by the OP crews as needed. Tidal energy shifts, besides being rather small, tend to average out over the duration of a run.

In addition to periodic tides the ring is also subject to slower seasonal circumference changes that were already observed at the time of LEP [10, 16]. Figure 16 displays the RF frequency adjustments that were made by the radial feedback to maintain the proton beams centered. The data in Figure 16 has been corrected for the tidal effects. The total frequency swing is 35 Hz, which corresponds to a circumference change of 2 mm and a relative energy variation of 2.6×10^{-4}.

In summary the contributions of energy variations over the year and other smaller corrections to the beam energy remain very small, a value of 3×10^{-4} can be considered as a conservative upper limit for the relative energy changes over a run above injection energy.

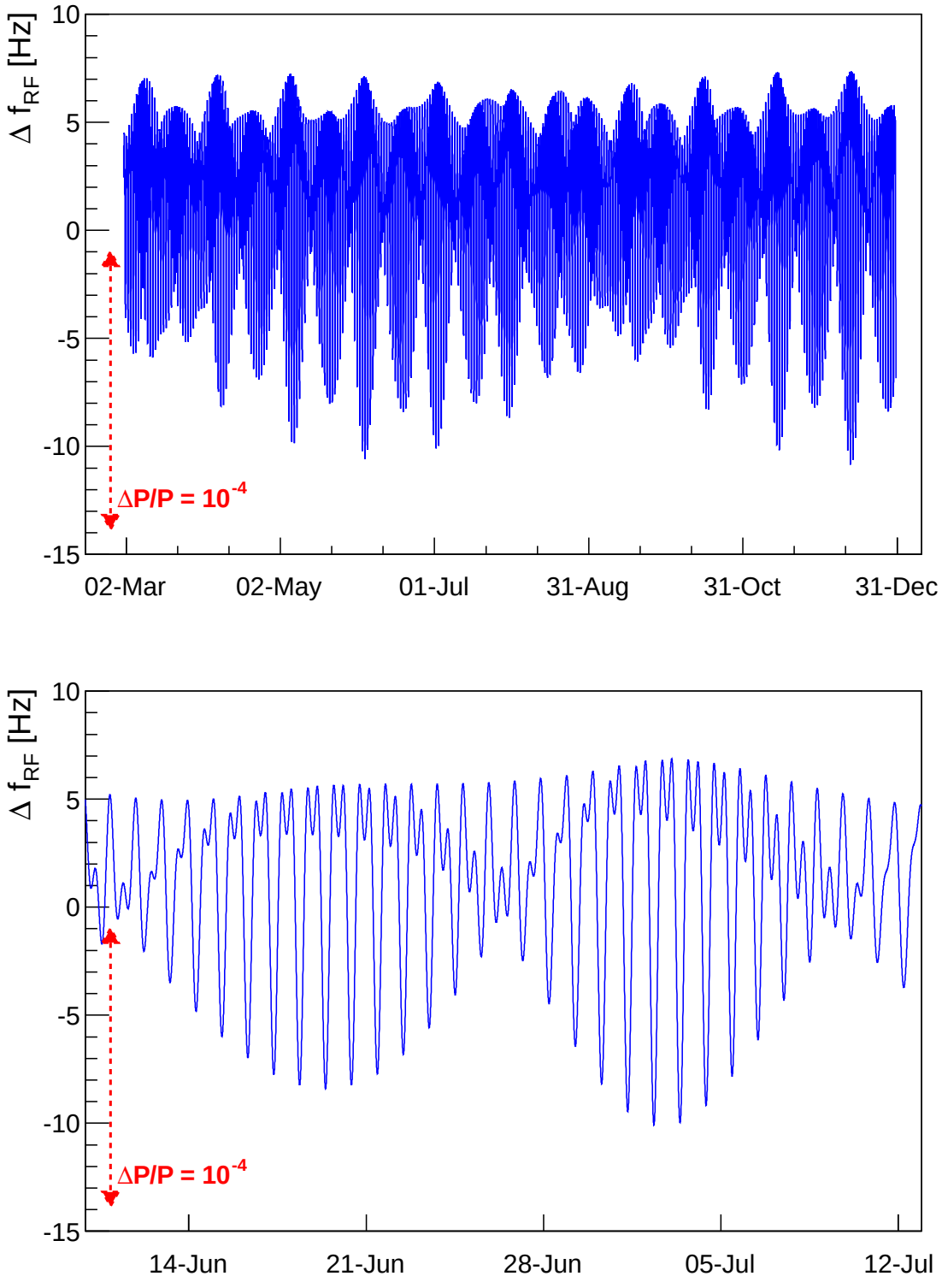

Figure 15: Change of RF frequency corresponding to the variation of circumference of the LHC ring due to Earth tides in 2012.

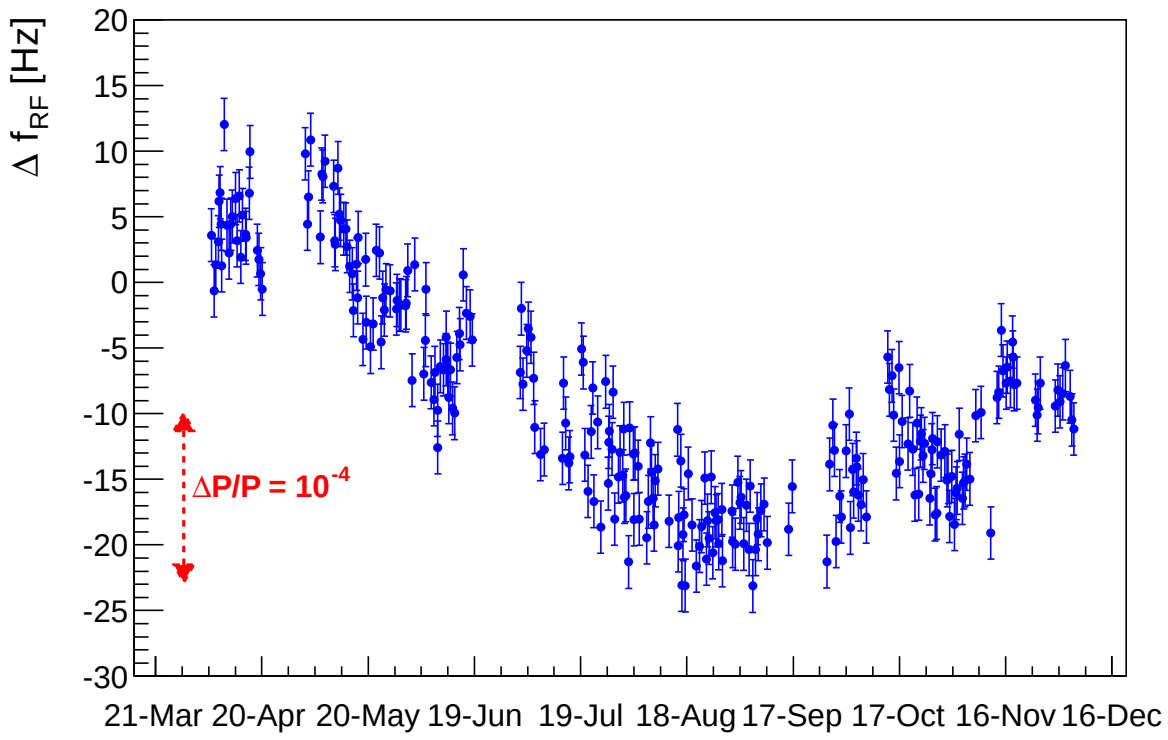

Figure 16: RF frequency changes required to center the beam in the BPMs at 4 TeV along the 2012 LHC run. The total change corresponds to a circumference change of 2 mm.

8.1 Energy Difference between the Rings and Centre-of-mass Energy

The main contributions to possible energy differences between the 2 rings are:

- differences in the integrated dipole field along the path of the beams,
- differences in the average beam position in the quadrupoles,
- differences in the horizontal orbit corrector settings.

The differences in integrated dipole field expected from the magnet measurements are smaller than 10^{-4} [19]. Such a difference may be estimated with beam data from the corrections that have to be applied to the trim quadrupoles to set the transverse tunes to their nominal values. This method only provides a rough estimate, since differences in gradient errors of the quadrupoles between the two rings are also a source of tune trim differences. The two other sources of energy differences (radial position and correctors) may also affect the total tune trims, but with a different sensitivity (natural versus total chromaticity). The 2012 run tune corrections at the top of the ramp yield a relative energy difference of less than 10^{-4} if derived from the vertical tune, and a possible difference of up to 7×10^{-4} based on the horizontal tune. The differences between the two planes tend to indicate that gradient errors contribute significantly to the tune trims. There are no indications that contradict the estimate of 10^{-4} for the relative energy difference obtained from the magnet measurements.

Taking into account the observed systematic differences between ring 1 and ring 2, and the very small offsets in the radial position of the two proton beams in p-p operation, the maximum difference in average radius is at the level of ± 3 Hz. This corresponds to a relative energy difference of $\pm 2 \times 10^{-5}$.

Energy offsets due to the orbit correctors can be determined directly from the settings of the orbit correctors. At 4 TeV a conservative upper limit for the difference is $\pm 10^{-4}$.

In summary, adding together all contributions, an upper limit for the relative energy difference between the 2 rings can be set to $\pm 2 \times 10^{-4}$.

At LEP the center-of-mass energy could differ significantly from one IP to the other due to the large synchrotron radiation loss and the unequal distribution of RF voltage around the machine circumference. This effect is completely negligible at the LHC due to the very small energy loss of only 6.7 KeV per turn even at 7 TeV. The energy loss scales $\propto E^4$).

Given that the energy differences between the two rings are very small compared to the measurement uncertainties and that there are no local energy shifts at the IPs, the centre-of-mass energy can be approximated as twice the beam energy. The relative errors on centre-of-mass energy and beam energy are identical since the energies of the two rings are essentially fully correlated.

9 Energy Extrapolations and Energy at 7 TeV

9.1 Uncertainty at other Energies

Between 2010 and 2012 the LHC was operated at 1.38, 3.5 and 4 TeV. No accurate p-Pb energy calibration is available at 1.38 and 3.5 TeV. The corrections that had to be applied to the machine (in particular the tune) do not exhibit signs of an unexpected beam energy error. Furthermore the 450 GeV calibration is in excellent agreement with the model (Section 7). For this reason the relative error of 0.65% obtained at 4 TeV (Equation (20)) can also be used for the LHC runs at 1.38 and 3.5 TeV. The nominal energy values of 1.38 TeV and 3.5 TeV should be used as central values. As discussed in the previous sections, the contributions due to differences of corrector settings and circumference variations are negligible at this level of accuracy.

9.2 Magnetic Extrapolation

The accurate energy measurement at injection can be extrapolated to higher energy using the magnet transfer functions. The uncertainty on the extrapolation is currently estimated to be $\delta_{int} = 7 \times 10^{-4}$ (relative error) [8, 18]. The measurement at injection presented in a previous section agrees within this uncertainty with the nominal energy.

The energy interpolation is performed using the simple equation

$$P_{int} = P_{\text{inj}} \, \frac{P_{ref}}{450[\text{GeV/c}]} \tag{25}$$

where P_{ref} is the nominal momentum. The momentum error is estimated using the relation

$$\sigma^2_{P,int} = (\delta_{int}(P_{ref} - 450[\text{GeV/c}]))^2 + \left(\sigma_{P,inj} \, \frac{P_{ref} - 450[\text{GeV/c}]}{450[\text{GeV/c}]}\right)^2 + (P_{int} - P_{ref})^2 \tag{26}$$

Reference Momentum P_{ref} (GeV/c)	Extrapolated Momentum P_{int} (GeV/c)	Momentum Error $\sigma_{P,int}$ (GeV/c)
450	450.28	0.11
1380	1380.9	1.1
3500	3502.2	3.2
4000	4002.5	3.7
6500	6504.0	6.1
7000	7004.4	6.6

Table 4: Extrapolated energies (from injection) and corresponding errors. The first line at 450 GeV is the reference point. The energy errors are based on a relative interpolation error of 7×10^{-4}.

$\sigma_{P,inj} = 0.11$ GeV/c is the error estimated for the measurement at injection, see Equation (23). The last term contributing to the error in Equation (26) takes into account the fact that it is not clear if the observed difference between measured and nominal energy at injection has to be scaled linearly to higher energy, or if it is an offset that only affects the low energies. The results of the interpolation are presented in Table 4. At 4 TeV the value agrees well with the direct measurement presented in this document.

9.3 Proton-Lead Measurements after Long Shutdown 1

After LS1 the LHC will be operated in the energy range of 6.5 to 7 TeV. A beam energy measurement using the technique applied at 4 TeV as described in the document would yield an uncertainty of ≈ 140 GeV/c at 7 TeV assuming the same total systematic error on the frequency measurement. Based on the experience of 2013 it seems possible to improve the systematic error by a factor 2 to 3 which would result in an error of $\approx 40-70$ GeV/c (0.5−1%). For a better control of the systematic errors, the measurement would profit from more frequent switching between p-Pb and Pb-p periods. While flipping every other fill is probably too heavy, it may be reasonable to split operation into two periods of p-Pb and two periods of Pb-p. Since this measurement requires a mixed p-Pb operation period, it is however unlikely to happen before the end of 2016.

Another possibility consists in interpolating the 4 TeV measurement presented in this document to 7 TeV as discussed in the previous section. This reduces significantly the lever arm with respect to injection energy.

10 Conclusions

The mixed proton and lead ion operation period was used to measure the beam energy at 4 TeV in an almost entirely parasitic way. The energy was obtained from the difference in radial position (and therefore speed) of the proton and lead beams. Even though the main aim was the measurement at 4 TeV, an accurate measurement was also performed at injection.

The result for the momentum at injection is

$$P_{\text{inj}} = 450.28 \pm 0.01\ (\text{stat})\ \pm 0.11\ (\text{syst})\ \text{GeV/c}\ , \tag{27}$$

while the momentum at 4 TeV is

$$P_{4\mathrm{TeV}} = 3988 \pm 5\ (\mathrm{stat})\ \pm 26\ (\mathrm{syst})\ \mathrm{GeV/c}\ . \tag{28}$$

Both measurements are dominated by the systematic errors. The relative uncertainty on the energy at 4 TeV is 0.65%. Since they are no signs of unexpected deviations of the magnetic fields in the machine data at 1.38 TeV and 3.5 TeV, the same 0.65% relative uncertainty applies also to those energies.

Within the quoted errors the energies of the two beams can be considered to be fully correlated.

Energy variations along the run and other contributions to the energy do not exceed $\pm 3 \times 10^{-4}$ in relative terms, i.e. $\pm$1.2 GeV/c. Similarly the relative energy difference between the two rings does not exceed $\pm 2 \times 10^{-4}$ or $\pm$0.8 GeV/c.

Using the magnetic model of the LHC and its estimated errors, the energy measurement at injection can be extrapolated to 4 TeV to yield

$$P_{4\mathrm{TeV,int}} = 4003 \pm 4\ (\mathrm{syst})\ \mathrm{GeV/c}\ . \tag{29}$$

which is in excellent agreement with the measurement presented in this document.

11 Acknowledgements

I thank the members of my section for their efficient operation of the LHC in the proton-lead period and for the dedicated calibration measurements that they performed for me. Without the work of John Jowett on the feasibility of the mixed proton lead operation, this measurement would not have been possible. I would like to thank Ezio Todesco for providing information and advice on the errors of the magnetic model of the LHC.

12 Appendix

Parameter	Symbol	Value
Proton mass [20] (MeV/c^2)	m_p	938.272046(21)
Electron mass [20] (MeV/c^2)	m_e	0.510998928(11)
Atomic mass unit [20](MeV/c^2)	m_u	931.494061(21)
Pb_{208} atomic mass [21]		207.976639(3)
Pb^{82+}_{208} atomic mass	m_{pb}/m_u	207.960730(3)
$\mu = m_{pb}/Zm_p$ ($Z = 82$, Eq. 10)		2.51743387(9)
Speed of light [20] (m/s)	c	299792458

Table 5: List of the fundamental parameters that are used to extract the beam momentum from the RF frequency measurements. The errors on the parameters are given in parenthesis. The atomic mass of Pb_{208} is corrected for the 82 missing electrons.

References

[1] ATLAS Collaboration, *Observation of a New Particle in the Search for the Standard Model Higgs Boson with the ATLAS Detector at the LHC*, **Phys. Lett. B 716** (2012) 1.

[2] CMS Collaboration, *Observation of a new boson at a mass of 125 GeV with the CMS experiment at the LHC*, **Phys. Lett. B 716** (2012) 30.

[3] G. Antchev *et al.*, *Luminosity-independent measurement of the proton-proton total cross section at* $\sqrt{s} = 8$ *TeV*, CERN-PH-EP-2012-354, accepted for publication in Phys. Rev. Letters.

[4] J. Jowett *et al.*, *p-Pb Feasibility Test and Modifications of LHC Sequence and Interlocking*, CERN-ATS-Note-2012-052 MD.

[5] J. Jowett *et al.*, *First proton-nucleus collisions in the LHC: the p-Pb pilot physics*, CERN-ATS-Note-2012-094 MD.

[6] J. Wenninger, *Beam Momentum Calibration at the LHC*, LHC Project Note 334, 2004.

[7] J. Wenninger, *Energy Calibration*, Proceedings of the LHC Lumi Days 2012, https://indico.cern.ch/conferenceOtherViews.py?view=standard&confId=162948

[8] L. Bottura, private communication.
L. Bottura et al., *Warm-Cold Magnetic Field Correlation in the LHC Main Dipoles*, LHC Project Note 326.

[9] R. Assmann *et al.*, *Calibration of centre-of-mass energies at LEP1 for precise measurements of Z properties*, **Eur. Phys. J. C 6** (1999) 2, 187-223.

[10] R. Assmann *et al.*, *Calibration of centre-of-mass energies at LEP2 for a precise measurement of the W boson mass*, **Eur. Phys. J. C 39** (2005), 253-292.

[11] R. Bailey *et al.*, Proc. of EPAC92, Nice, France.

[12] X. Altuna *et al.*, *A Momentum Calibration of the SPS Proton Beam*, CERN SL/92-32.

[13] G. Arduini *et al.*, *Energy Calibration of the SPS at 450 GeV/c with Proton and Lead Ion Beams*, AB-Note-2003-014 OP.

[14] L. Arnaudon *et al.*, Nucl. Instr. Meth. A 357, 249 (1995).

[15] J. Wenninger, *Radial deformations of the LEP ring*, CERN SL/Note 95-21 OP.
J. Wenninger, *Observation of radial ring deformations using closed orbits at LEP*, Proc. of PAC99, New York.

[16] J.Wenninger, *Orbit Steering and Central Frequency for LEP2 Energy Calibration*, SL-Note-2000-09 OP.

[17] E. Calvo-Giraldo *et al.*, *The LHC Orbit and Trajectory System*, CERN-AB-2003-057 BDI and Proceedings of the 6th European Workshop on Beam Diagnostics and Instrumentation for Particle Accelerators, Mainz, Germany, 5-7 May 2003, pp.187.

[18] E. Todesco *et al.*, *The Magnetic Model of the LHC during the 3.5 TeV Run*, Proceedings of IPAC12, New Orleans, May 2012.

[19] E. Todesco, private communication.

[20] J. Beringer *et al.* (Particle Data Group), **Phys. Rev. D86**, 010001 (2012) http://pdg.lbl.gov/

[21] G. Audi and A.H. Wapstra, **Nucl. Phys A595**, 409 (1995).